

MODELING OF THE CHEMICAL X-PARAMETER IN PSEUDOBINARY ALLOYS FROM THE SHIFT OF THE X-RAY BRAGG ANGLE: APPLICATION TO CUBIC $Ba_xSr_{1-x}TiO_3$ FILMS

K. A. AGUILAR CRUZ^a, J. J. MEDEL JUÁREZ^a,
M. T. ZAGACETA ÁLVAREZ^b, R. PALMA OROZCO^c,
F. CABALLERO-BRIONES^d, J. L. FERNÁNDEZ-MUÑOZ^{e,*}

^aComputer Research Center, National Polytechnic Institute (CIC-IPN), Juan de Dios Bátiz Avenue, Esq. Miguel Othón de Mendizábal, Col. Nuevo Vallejo Industrial, Gustavo A. Madero, Z.P. 07738 México City, Mexico

^bHigher School of Mechanical and Electrical Engineering (ESIME-IPN-AZ), Azcapotzalco Unit, National Polytechnic Institute, Av. Granjas, Mexico City, Z.P. 02250, Mexico

^cSchool of Computing, National Polytechnic Institute (ESCOM-IPN), Av. Juan de Dios Bátiz Avenue, Corner Miguel Othón de Mendizábal, Col. Lindavista, Gustavo A. Madero, Z.P. 07738 Mexico City, Mexico

^dNational Polytechnic Institute, Materials and Technologies for Energy, Health and Environment (GESMAT), CICATA-IPN Altamira Unit; Km 14.5 Carretera Tampico-Puerto Industrial Altamira, Z.P. 89600 Altamira, Tamaulipas Mexico

^eNational Polytechnic Institute, Materials and Technologies for Energy, Health and Environment (GESMAT), CICATA-IPN Legaria Unit, Legaria 694 Avenue, Col Irrigación, Z.P. 11500 Mexico City, Mexico

Pseudobinary alloys of the type $A_xB_{1-x}C$ are expected to obey the Vegard's law that states a linear relationship between the chemical parameter x and the lattice parameter. However, in many cases, deviations from the Vegard's are found, and the calculation of x requires compositional characterization, often complicated in the presence of secondary phases of the same material. In the present work, $Ba_xSr_{(1-x)}TiO_3$ (BSTO) films were deposited by RF co-sputtering from $BaTiO_3$ and $SrTiO_3$ targets to obtain differently Ba/Sr ratios considering the different RF-power applied to each target. We describe a mathematical model based on the Boltzmann equation to calculate the x parameter of the cubic phase of the BSTO films in the $0 \leq x \leq 1$ range. That was made by following the 2θ diffraction angular shift of the plane (111) upon the increase of substitutional Ba^{2+} in the pseudobinary alloy, as a function of the RF applied power and fitting the interplanar distances and lattice parameter in the alloys were calculated onto the fitted sigmoid trajectory. The model showed the region where the lattice parameter a vs x obeys the Vegard's law and correctly fitted "a" in the entire $0 < x < 1$ range. The model can be applicable to other pseudobinary systems with deviations from the Vegard's law, from a simple X-ray diffraction analysis, providing fast chemical information, complementary with further compositional characterization.

(Received September 10, 2019; Accepted January 17, 2020)

Keywords: Sputtering deposition, Thin films, Stoichiometric behavior, Barium strontium titanate, Boltzmann's Equation.

1. Introduction

Pseudobinary alloys of the form $A_xB_{1-x}C$ tend to follow the Vegard's law, i.e. the lattice parameter varies linearly with the x -composition parameter, allowing the calculation of x from the lattice parameter obtained from X-ray diffraction [1,2]. However, early works have reported deviations from the Vegard's law in several pseudobinary alloys, leading to S-shaped or

* Corresponding author: jlfernandez@ipn.mx

negative/positive bowing at compositions close to $x \approx 0$ or $x \approx 1$ [1-3]. These tendencies have been satisfactorily explained by covalent bond-bending forces in the case of the S-shaped deviation, or by bond stretching in the case of the bowing of the lattice parameter or energy bandgap vs x [2]. Therefore, the modelling and prediction of the x -parameter values using only the diffraction values without knowing the experimental behavior of a vs x for a given system is not, *a priori*, straightforward. An approach that has been proposed to calculate the x -parameter in systems that present bowing in a vs x plots, include the introduction of a fitting parameter in a quadratic expression of the type:

$$Eg(x) = (1 - x)Eg_{AC} + xEg_{BC} - bx(1 - x)$$

where Eg is the variation of the calculated energy bandgap of the alloy with the alloy composition x , AC and BC are the binary compounds of the $A_xB_{1-x}C$ alloy and b is the bowing parameter. However, to the best of our knowledge, any model is published to predict x in systems presenting the S-shaped deviation from Vegard's law.

$Ba_xSr_{(1-x)}TiO_3$ (BSTO) films have several applications in solar cells, photo-catalysis, resistive memories, sensors, and so on [4-12]. BSTO films and powders have been prepared by several techniques such as arc discharge, sol-gel, pulsed laser deposition, hydrothermal reaction, chemical synthesis, molecular beam epitaxy and co-sputtering [4-12]. The BSTO functional properties such as the ferroelectric parameters and the optical band gap depend on the x -parameter that defines the chemical composition [13-18]. In our previous works, BSTO thin films, have been prepared by co-sputtering from $BaTiO_3$ (BTO) and $SrTiO_3$ (STO) targets, varying the applied power to each magnetron [12, 18]. During the progressive substitution of Ba with Sr into BSTO a lattice contraction was inferred from the Bragg angle shift, [18]. The lattice parameter as function of the x -parameter obtained from energy-dispersive X-ray spectra (EDS) showed an S-shaped deviation from Vegard's law [19,20]. The data were fitted with a Boltzmann-like function that depends on the sputtering parameters, that allowed inferring an empirical relationship between the applied power, with the film properties, including the composition [18-20].

The present work proposes a general model that considers the values of x as a function of the Bragg angle for a given set of diffraction peaks. The model shall be applicable to other pseudobinary alloys that exhibit an S-deviation behavior in its lattice parameter vs x , to permit a simple calculation of the alloy stoichiometry.

2. Experimental details

BSTO films were prepared by RF magnetron sputtering in a system equipped with two magnetrons: $BaTiO_3$ (BTO, 99.95%, SCI Engineered Materials Inc) and $SrTiO_3$ (STO, 99.9%, SCI Engineered Materials Inc.). Targets were 2" diameter and 0.125" thick. Before film deposition, the sputtering chamber was evacuated to a base pressure around 1.2×10^{-3} Pa; then, an Ar flushing was done filling the chamber to a pressure of 3.9 Pa during 10 minutes. For the film deposition, an Ar + O₂ gas mixture was introduced into the chamber with an Ar/O₂=90/10 ratio at an initial pressure of 6.6 Pa to ignite the plasma and perform a target pre-sputtering during 15 minutes. After that, the working pressure was set at 3.9 Pa to carry out the deposition. Quartz substrates 1 x 1 cm² were successively rinsed with trichloroethylene, acetone, and ethanol before depositing. A stainless-steel substrate holder was fixed at a distance of 8 cm from the magnetron in off-axis configuration. The substrate holder was rotated at 100 rpm for ensuring film uniformity and the substrate temperature was set at 549°C. The total applied RF-magnetron power was 120 watts, distributed between the two magnetrons as shown in Table 1, in order to produce $Ba_xSr_{1-x}TiO_3$ films with different stoichiometric compositions. The sputter time for all of samples was 68 minutes. The X-ray diffractograms were acquired in a Phillips X'Pert diffractometer using Cu K α =1.54060 Å.

Table 1. RF power applied at the individual $SrTiO_3$ and $BaTiO_3$ targets. Total applied power was 120 W.

Sample	Applied power (W)	
	BaTiO ₃	SrTiO ₃
M1	120	0
M2	105	15
M3	90	30
M4	75	45
M5	60	60
M6	45	75
M7	30	90
M8	15	105
M9	0	120

3. Mathematical Model

In a previous study, we have found that the x parameter in $Ba_xSr_{(1-x)}TiO_3$ films with cubic structure as a function of the plasma power applied to the BaTiO₃ target follows a sigmoidal profile close to Equation (1), *i.e.* the Boltzmann equation [8-11].

$$y(x) = y_f - \left[\frac{(y_f - y_i)}{A + e^{\frac{x-c}{\alpha}}} \right] \quad (1)$$

where y_i is the minimum asymptote, and y_f is the maximum asymptote on the y-axis; c corresponds to the inflection point in the sigmoidal curve; α is a coefficient that describes the slope behavior during the transition, and A is a fitting parameter.

In the present contribution, we further refine the basic Boltzmann model and propose Equation (2) as a mathematical model to calculate the x -composition parameter directly from the RF power applied to the BaTiO₃ target, based on our previous works:

$$x(P_i) = x_f - \left[\frac{(x_f - x_i)}{1 + e^{\frac{(P_i - P_0)}{\alpha}}} \right] \quad (2)$$

Here, x is the chemical parameter in $Ba_xSr_{(1-x)}TiO_3$, P_i is the RF power applied to the BaTiO₃ target, where the values used in the above-described experiment were 0, 15, 30, 45, 60, 75, 90, and 120 W; P_0 is the applied power when $x = 0.5$, and α (applied power units) is a coefficient that describes the behavior of the slope value during the transition line from x_i to x_f values that correspond to the initial and the final values of x in the $Ba_xSr_{(1-x)}TiO_3$ alloy, *i.e.* 0 and 1 respectively. Therefore, $x'(P_i)$ Equation (3), and $x''(P_i)$, Equation (4) represent the first and second derivatives of Equation (2), respectively:

$$\frac{d}{dP_i} x(P_i) = \frac{1}{\alpha^2} \left[\frac{(x_f - x_i) e^{\frac{(P_i - P_0)}{\alpha}}}{\left(1 + e^{\frac{(P_i - P_0)}{\alpha}}\right)^2} \right] \quad (3)$$

$$\frac{d^2}{dP_i^2} x(P_i) = \frac{(x_f - x_i) e^{\frac{(P_i - P_0)}{\alpha}}}{\alpha^2 \left(1 + e^{\frac{(P_i - P_0)}{\alpha}}\right)^2} \left\{ 1 - \frac{2e^{\frac{(P_i - 46)}{14.4}}}{1 + e^{\frac{(P_i - 46)}{14.4}}} \right\} = - \frac{(x_f - x_i) e^{\frac{(P_i - P_0)}{\alpha}}}{\alpha^2 \left(1 + e^{\frac{(P_i - P_0)}{\alpha}}\right)^2} \tanh \left[\frac{P_i - P_0}{2\alpha} \right] \quad (4)$$

The first derivative has a maximum in $x'(P_0) = \frac{(x_f - x_i)}{2\alpha}$ and $x(P_0) = \frac{(x_f + x_i)}{2}$; . The second derivative considers the minimum gradient value when $x''(P_0) = 0$.

Bragg's law: $d_i = \frac{n\lambda}{2\sin(\theta_i)}$ was used to calculate the interplanar distance; where: n is an integer, λ is the wavelength of X-rays, d_i is the distance between the planes of the crystalline lattice and, θ_i is the angle between the incident rays and the scattering planes. From the d values, the lattice parameter a for the cubic phase was calculated from: $\frac{1}{d^2} = \frac{h^2+k^2+l^2}{a^2}$.

4. Results and discussion

Fig. 1 depicts the evolution of the Bragg angles of the (111) plane, for the films prepared at different plasma power at the BTO target. The (111) peaks of the pure c-BaTiO₃ and c-SrTiO₃ are indicated in the Figure, while the evolution of the (111) peak to lower diffraction angles within the applied power is clearly observed. The corresponding values of the Bragg peaks and the interplanar distances, d , and lattice parameter, a , are presented in Table 2. The shift of the Bragg peak to lower angles indicates the lattice expansion due to the Ba²⁺ incorporation into the Sr²⁺ sites, as the values in Table 2 confirm.

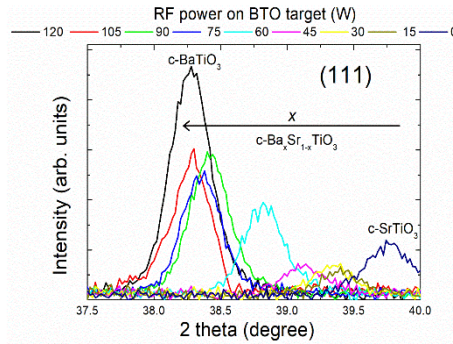


Fig. 1. Values of the peak diffraction angles corresponding to the plane (111) for the samples in Table 1.

Table 2. Parameters for the 2θ diffraction angles of the (111) plane, inter-planar distance (d) \AA , lattice parameter (a) \AA , and cell volume \AA^3 at the different power applied to the BTO target.

Power at BTO target	Bragg's angles $2\theta(111)$	d (111)	a (111)	Volume (111)
120	38.28	2.355	4.078	67.826
105	38.32	2.352	4.074	67.622
90	38.34	2.351	4.072	67.52
75	38.4	2.347	4.066	67.216
60	38.58	2.337	4.048	66.315
45	38.84	2.322	4.022	65.042
30	39.1	2.307	3.996	63.803
15	39.3	2.296	3.976	62.872
0	39.4	2.29	3.967	62.413

Fig. 2 shows the evolution of the 2θ values for the (111) plane as a function of the RF power applied at the BTO target. The figure also shows the fitting using Equation 2. A similar analysis was done for the displacement observed in 2θ diffraction angles associated with the (110) and (211) planes of the cubic phase, as well as for the peaks of the tetragonal and orthorhombic phases, finding similar results (not presented).

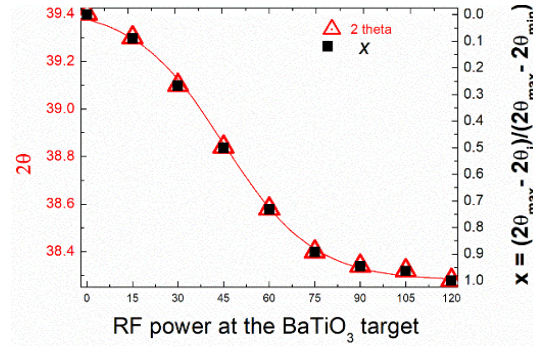


Fig. 2. Experimental data and fitting of the 2θ values for the (111) plane of the prepared films as a function of the RF power applied at the BTO target. The right vertical axes indicate the relationship between the x parameter and 2θ diffraction angles, calculated from the model.

The $2\theta_i$ vs P_i the plot in Fig. 2 was fitted by substituting x_i to x_f by $2\theta_{min}$ and $2\theta_{max}$ in Equation 2 to obtain the Equation (5):

$$2\theta_i = 39.4 - \frac{1.12}{1 + e^{\frac{(P_i - 45.36)}{14.064}}} \quad (5)$$

where $2\theta_{min} = 38.28$, $2\theta_{max} = 39.4$ and $2\theta_{max} - 2\theta_{min} = 1.12$. The $2\theta_{min}$ and $2\theta_{max}$ experimental values were taken of Table 2.

Therefore, Equation (5) takes the general form:

$$\frac{2\theta_i - 2\theta_{min}}{2\theta_{max} - 2\theta_{min}} = \left[\frac{1}{1 + e^{\frac{(P_i - 45.36)}{14.06}}} \right] \quad (6)$$

Equation (6) has the same mathematical form than Equation (2); thus it represents the x parameter calculated from the shift in the $2\theta_i$ values. When $x_f = 1$, $x_i = 0$, $P_0 = 45.36$, $\alpha = 14.064$ values are substituted in the Equation (2) to get Equation (7).

$$\left[\frac{1}{1 + e^{\frac{(P_i - 45.36)}{14.06}}} \right] = 1 - x \quad (7)$$

If Equation (7) is evaluated at $P_{i=0} = 45.36$, the result is $x = 0.5$; therefore, Equation (6) represents the sigmoidal profile of the evolution of the x value calculated from the Bragg angles.

By calculating the interplanar distances from the Bragg law, Equation (7) takes the form:

$$\frac{d_{max} - d(P_i)}{d_{max} - d_{min}} = \left[\frac{1}{1 + e^{\frac{(P_i - 46)}{14.4}}} \right] = 1 - x \quad (8)$$

where: $d_{max} = 2.355 \text{ \AA}$, $d_{min} = 2.29 \text{ \AA}$ and $d_{max} - d_{min} = 0.065 \text{ \AA}$, Fig. 3 presents the evolution of the interplanar distance as a function of the RF-power applied to the BTO target. The experimental data were fitted with Equation (8). Thus, the simplest sigmoidal model to describe the interplanar distance evolution within the applied power, is determined uniquely by three points: the top value $d = 2.335 \text{ \AA}$, corresponding to the (111) interplanar distance of BaTiO_3 the bottom value $d = 2.29 \text{ \AA}$ of the interplanar distance between the (111) planes of SrTiO_3 , and the midpoint or transition point when $x = 0.5$, obtained at an applied power of 46 W, with a $d = 2.31 \text{ \AA}$. Fig. 4 presents the first derivative of Equation 8, where the maximum value at an applied power of 45 W, represents the highest variation of the interplanar distance, *i.e.*, when the $\text{Ba}_x\text{Sr}_{(1-x)}\text{TiO}_3$ alloy has a stoichiometric equilibrium ratio for $\text{Ba}/\text{Sr} = 1$ or $x = 0.5$.

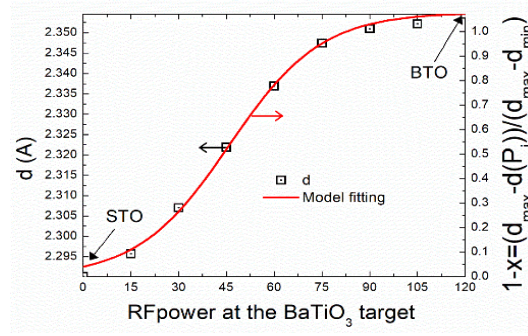


Fig. 3. Inter-planar distance d as a function of RF power at the BTO target. The right vertical axis shows the mathematical model relating d and x parameter respectively.

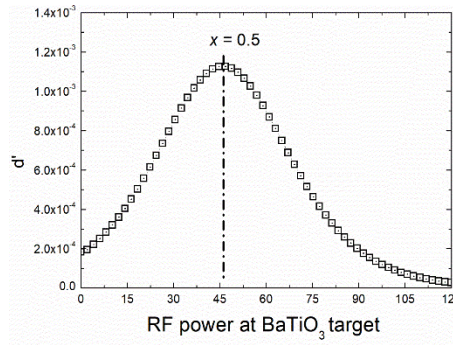


Fig. 4. The first derivative of Equation (8) as a function of RF-power applied at the BTO target.

The shape of the derivative curve shows that the interplanar distance increases faster when Ba content increases at $x < 0.5$ and slower from $x > 0.5$, possibly because structural impediment to incorporate more Ba in the stressed lattice. When evaluated at the applied plasma power of 46 W, Equation (9), is obtained.

$$d'(P_i) = \frac{d}{dP_i} \left[d_{max} - \frac{(d_{max} - d_{min})}{1 + e^{\frac{P_i - 46}{14.4}}} \right] = \frac{0.065}{14.4} \left[\frac{e^{\frac{P_i - 46}{14.4}}}{\left(1 + e^{\frac{P_i - 46}{14.4}}\right)^2} \right] \quad (9)$$

and $d'(P_0) = \frac{0.065 \text{ \AA}}{28.8 \text{ W}} = 0.00225 \frac{\text{Å}}{\text{W}}$, it is the top variation of the interplanar distance. To further analyze the behavior of the interplanar distance, Equation (10) represents the second derivative of Equation (3), evaluated with the parameters found in Equation (8).

$$d''(P_0) = \frac{0.065 e^{\frac{P_i - 46}{14.4}}}{207.36 \left(1 + e^{\frac{P_i - 46}{14.4}}\right)^2} \left\{ 1 - \frac{2e^{\frac{P_i - 46}{14.4}}}{1 + e^{\frac{P_i - 46}{14.4}}} \right\} = -\frac{0.00031 e^{\frac{P_i - 46}{14.4}}}{\left(1 + e^{\frac{P_i - 46}{14.4}}\right)^2} \tanh \left[\frac{P_i - 46}{28.8} \right] \quad (10)$$

Fig. 5A presents the plot of Equation 10, d'' vs. the applied RF-power. The inflection point at 46 W corresponds to $x=0.5$ as mentioned above. The region between 32 W and 62 W indicates that the interplanar distance varies linearly with the composition, *i.e.* follows the Vegard's law. The positive region of d'' represent Ba^{2+} incorporation at $x < 0.5$ and the negative region, the Ba^{2+} incorporation from $x > 0.5$. On the other hand, Fig. 5B shows the evolution of the

lattice parameter a vs the applied power. The region from 32 W to 62 W was fitted linearly vs the applied power; the resultant expression was $a = 0.00173(P_i) + 3.944$.

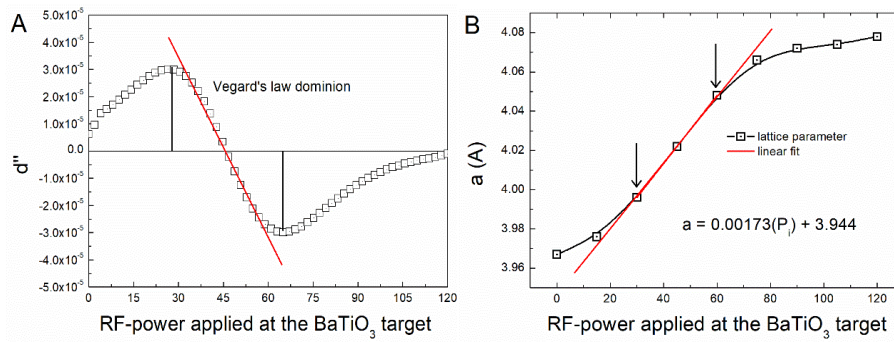


Fig. 5. A) The second derivative of Equation (8) and B) lattice parameter a , as a function of RF-power applied to the $BaTiO_3$ target.

Fig. 6 presents the scale transformation from applied power to 2 theta for the (111) plane of the BSTO films, taken from Fig. 2, to calculate the x parameter using the Boltzmann-like model proposed here. The results indicate the model is capable of adjusting the structure of the entire compositional range $0 < x < 1$, providing a tool to calculate the x parameter in pseudobinary alloys, even they are out of the Vegard's law. As mentioned in the introduction, there are no models published for the S-type deviation of the Vegard's law [1,2], while for quadratic deviations, the bowing parameter model fits quite well.

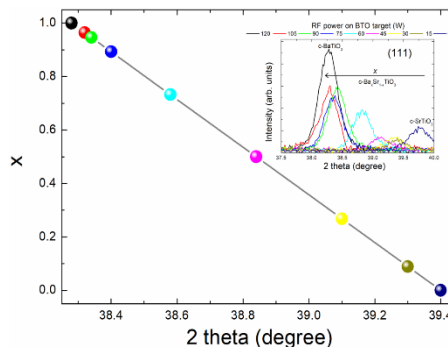


Fig. 6. x -parameter vs 2 theta plot obtained from the scale transformation of Figure 2. The inset presents the evolution of the 2 theta position for the (111) plane of the cubic BSTO films.

5. Conclusions

A simple mathematical model based on the Boltzmann equation was proposed to obtain chemical information from the relationship between the shift of the 2θ diffraction angles in X-ray diffractograms, and the x parameter in pseudobinary alloys of the type $A_xB_{1-x}C$ when $0 \leq x \leq 1$ which present an S-deviation from the Vegard's law. The model was tested in $Ba_xSr_{(1-x)}TiO_3$ (BSTO) films deposited by RF co-sputtering from $BaTiO_3$ and $SrTiO_3$ targets. The lattice parameter vs the x -parameter of the deposited films does not obey the Vegard's law at $x < 0.73$ and $x > 0.95$; however, the model successfully fitted the lattice parameter in the entire x -range. The first and second derivatives of the model provide some structural information such as the substitution dynamics of Ba^{2+} substitution in Sr^{2+} sites, although further work is intended to refine the model in this direction.

The merit of the present model consists in the calculation of the chemical parameter x in pseudobinary systems that do not necessarily obey the Vegard's law, by following the evolution of

the diffraction peak position in the entire composition range. The model needs only either the experimental or reported 2θ positions for the compounds with $x=1$ and $x=0$ values of an $A_xB_{1-x}C$ alloy and the experimental 2θ position of at least one intermediate point with composition $0 < x < 1$.

Acknowledgments

FCB and JLFM acknowledges the financial support from SIP-IPN project 20194931-6350.

References

- [1] N. R. Short, *J. Phys. D: Appl. Phys.* **1**, 129 (1968)
- [2] C. Y. Fong, W. Weber, J. C. Phillips, *Phys. Rev. Phys* **14**, 5387 (1976).
- [3] S. W. Kang, Y. Y. Kim, C. H. Ahn, S. K. Mohanta, H. K. Cho, *J. Mater. Sci: Mater. Electron.* **19**, 755 (2008)
- [4] J. C. Agar, S. Pandya, R. Xu, A. K. Yadav, Z. Liu, T. Angsten, S. Saremi, M. Asta, R. Ramesh. *MRS Commun.* **6**, 151 (2016).
- [5] U. Gleissner, C. Megnin, M. Benkler, D. Hertkorn, H. C. Elsenhmeier, K. Schumann, F. Paul, T. Hanemann, *Ceram-Silikáty* **60**, 1 (2016).
- [6] E. Yustanti, M. Ayu, E. Hafizah, A. Manaf, *AIP Conference Proceedings* **1725**, 020102 (2016).
- [7] H. Kojima, M. Watanabe, I. Tanaka, *Journal of Crystal Growth* **155**, 70 (1995).
- [8] B. Wu, L. Zhang, X. Yao, *Ceramics International* **30**, 1757 (2004).
- [9] S. B. Deshpande, Y. B. Kholam, S. V. Bhoraskar, S. K. Date, S. R. Sainkaa, H. S. Potdar, *Materials Letters* **59**, 293 (2005).
- [10] Y. B. Kholam, H. S. Potdar, S. B. Deshpande, A. B. Gaikwad, *Materials Chemistry and Physics* **97**, 295 (2006).
- [11] F. Alema, A. Reinholz, K. Pokhodnya, *J. Appl. Phys.* **114**, Article ID174104, (2013).
- [12] J. Reséndiz-Muñoz, J. L. Fernández-Muñoz, J. R. Farias-Mancilla, M. Melendez-Lira, J. J. Medel-Juárez, O. Zelaya-Angel, *Digest Journal of Nanomaterials and Biostructures* **13**, 751018).
- [13] S. Das, D. Liu, V. Janardhanam, C.-J. Choi, Y.-B. Hahn, *RSC Adv.* **2**, 10255 (2012).
- [14] A. El Ghandouri, S. Sayouri, T. Lamcharfi, L. Hajji, *Environ. Sci.* **8**, 4945 (2017).
- [15] P. Kumar, S. Singh, J. K. Juneja, C. Prakash, K. K. Raina, *Physica B* **404**, 1752 (2009).
- [16] P. Kumar, S. Singh, M. Spah, J. K. Juneja, C. Prakash, K. K. Raina, *Journal of Alloys and Compounds* **489**, 59 (2010).
- [17] M. Sindhu, N. Ahlawat, S. Sanghi, R. Kumari, A. Agarwal, *Journal of Alloys and Compounds* **575**, 109 (2013).
- [18] J. Reséndiz-Muñoz, J. Estrada-Martínez, M. Á. Meléndez-Lira, O. Zelaya-Ángel, J. J. Medel-Juárez, F. Caballero-Briones, J. L. Fernández-Muñoz, *Coatings* **8**, 362 (2018).
- [19] J. Reséndiz-Muñoz, M. A. Corona-Rivera, J. L. Fernández-Muñoz, M. Zapata-Torres, A. Márquez-Herrera, V. M. Ovando-Medina, *Bulletin of Materials Science* **40**, 1043.
- [20] J. Reséndiz-Muñoz, J. L. Fernández-Muñoz, M. A. Corona-Rivera et al., *Journal of Nanomaterials* **2017**, Article ID 4308294, 8 pages, (2017).